Advances in Aircraft and Spacecraft Science, *Vol. 6, No. 1 (2019) 019-030*
DOI: https://doi.org/10.12989/aas.2019.6.1.019

Shock wave instability in a bent channel with subsonic/supersonic exit

Alexander Kuzmin*

Department of Fluid Dynamics, St. Petersburg State University, 28 University Avenue, 198504, Russia

(Received July 4, 2018, Revised September 10, 2018, Accepted September 13, 2018)

Abstract. Two- and three-dimensional turbulent airflows in a 9-degrees-bent channel are studied numerically. The inner surfaces of upper and lower walls are parallel to each other upstream and downstream of the bend section. The free stream is supersonic, whereas the flow at the channel exit is either supersonic or subsonic depending on the given backpressure. Solutions of the Reynolds-averaged Navier-Stokes equations are obtained with a finite-volume solver ANSYS CFX. The solutions reveal instability of formed shock waves and a flow hysteresis in considerable bands of the free-stream Mach number at zero and negative angles of attack. The instability is caused by an interaction of shocks with the expansion flow formed over the convex bend of lower wall.

Keywords: shock waves; curved channel; instability; hysteresis; turbulent boundary layer

1. Introduction

Supersonic airflow in convergent and convergent-divergent channels is known to be unstable (Sforza 2012). The instability triggers the swallowing and expulsion of shocks with variations of free-stream Mach number M_∞ or the angle of attack α if the channel contraction ratio is moderate enough. A classical interpretation of the instability in convergent channels is based on quasi-one-dimensional equations governing mass flow rate and stagnation temperature across the normal shock (Torenbeek and Wittenberg 2009).

Recently, shock wave instability was revealed in monotonously divergent bent channels (Kuzmin 2015, 2016). In this case, a shock wave arises due to a concave bend/corner of a wall, whereas its instability is caused by an interaction with the convex bend of the opposite wall. Numerical simulations demonstrated a flow hysteresis and jumps of shock positions with gradual variations of M_∞ or α.

A similar problem was explored by Guo *et al.* (2014) where numerical modeling of supersonic flow in a curved channel of nearly constant cross-section showed the existence of a flow hysteresis with variations of the given outlet pressure.

In practice, curved channels are utilized, e.g., in Y-shaped intakes of battle-plane and fighter aircraft engines. Kotteda and Mittal (2016) studied the effect of sideslip angle on the performance of a slightly divergent Y-intake at various back pressure ratios. Different flow regimes as a result of these variations were identified, and an effect of the initial condition was investigated as well.

*Corresponding author, Dr.Sc., E-mail: a.kuzmin@spbu.ru

 ISSN: 2287-528X (Print), 2287-5271 (Online)

Supersonic flow in curved channels is also of interest for the design of rampressors, which are compressors operating at high peripheral speeds necessary to achieve supersonic effect in a stationary environment. Han *et al*. (2009) and Kang *et al*. (2014) investigated the performance of rampressors and flow excitation characteristics under different frequencies and amplitudes of rampressor rotor whirling.

Feng *et al*. (2017a, b) performed a numerical and experimental study of supersonic flow in a bent channel which models a variable geometry dual mode combustor. The study indicated that the static pressure distribution on the wall had an obvious hysteresis phenomenon with continuous variations of the wedge position governing the outlet cross section area.

Kuzmin (2017) examined the flow instability in a channel with a short upper wall (cowl) which was set at various inclination angles to the lower wall. Positive, negative and zero inclination angles were considered, and interactions of the arising shocks were examined. At the channel exit we used a condition of the supersonic flow regime.

In the present paper, we deal with a channel whose walls are parallel before and after the bend section. Therefore, the channel at hand is neither divergent, nor convergent. Considerable attention is paid to a subsonic flow condition at the exit, which admits smaller supersonic regions in the channel than those in (Kuzmin 2017). In Sections 2 and 3 we formulate the problem and outline a numerical method. Then in Sections 4 and 5 we study a dependence of 2D shock positions on M_∞ at zero and negative angles of attack. Finally, in Section 6 we discuss effects of the Reynolds number and 3D phenomena on the flow.

2. Formulation of the problem for 2D flow

Let us consider a channel whose lower wall is an expansion corner

$$y=0 \quad \text{at} \quad -60 \le x \le 0, \qquad y=-x\tan 9^\circ \qquad \text{at} \qquad 0 \le x \le 50, \tag{1}$$

whereas the upper wall is a compression corner

$$y=30 \quad \text{at} \quad -28 \le x \le 0, \qquad y=30-x\tan 9^\circ \qquad \text{at} \quad 0 \le x \le 50 \tag{2}$$

see Fig. 1. Here and further in the paper, the Cartesian coordinates (x,y,z) are dimensional and given in millimeters. The thickness of leading edges of the upper and lower walls is 0.05. The outer surfaces of the lower and upper walls are a segment and corner, respectively.

The inflow boundary Γ_{in} of the computational domain is formed by two segments with the beginnings at the point $y=0$, $x= -65$ and ends at $x= 15$, $y= \pm 170$. We prescribe the x-, y- and z-components of the velocity on Γ_{in} as follows:

$$U_\infty = M_\infty a_\infty \cos\alpha, \qquad V_\infty = M_\infty a_\infty \sin\alpha, \qquad W_\infty = 0 \tag{3}$$

In addition, we impose on Γ_{in} the static pressure p_∞, the turbulence level of 1%, and static temperature T_∞=200 K which determines the sound speed a_∞=283.58 m/s.

The outflow boundary Γ_{out} of the computational domain is constituted by two segments with the beginnings on the outer surfaces of walls at x=30 and ends x=15, y=±170. We prescribe the condition $M>1$ on Γ_{out}. At the channel exit x=50 we impose either the supersonic condition $M>1$ or subsonic one with a given pressure p_{exit}. The vanishing heat flux and no-slip condition are imposed on the walls. The air is treated as a perfect gas whose specific heat at constant pressure is 1004.4 J/(kg K) and the ratio of specific heats is 1.4. We use the Sutherland formula for the molecular dynamic viscosity and adopt the value of 28.96 kg/kmol for the molar mass. The

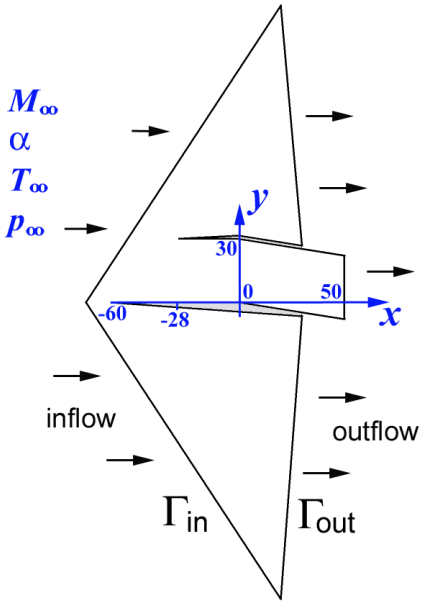

Fig. 1 Sketch of the computational domain in the plane (x,y)

pressure p_∞ is set to 4×10^4 N/m^2 throughout the paper, except for Fig. 11 in which we compare results obtained for smaller and larger pressures. The Reynolds number based on $p_\infty=4\times10^4$ N/m^2, $M_\infty=1.3$, and height of the channel is 5.75×10^5. Initial data are either parameters of the free stream or a flow field calculated for a different M_∞.

3. Numerical method

Solutions of the unsteady Reynolds-averaged Navier-Stokes equations were obtained with an ANSYS-18.2 CFX finite-volume solver of second-order accuracy. An implicit backward Euler scheme was employed for the time-accurate computations. We used a curvature corrected Shear Stress Transport k-ω turbulence model, which is known to reasonably predict aerodynamic flows with boundary layer separations (Spalart and Shur 1997, Menter 2009).

Simulations of the 2D flow were performed on hybrid unstructured meshes constituted by quadrangles in 38 layers on the walls and by triangles in the remaining region, see Fig. 2. The non-dimensional thickness y^+ of the first mesh layer on the walls was less than 1. The sizes of triangles essentially decreased in the channel for an accurate resolution of shock waves. Test solutions obtained on uniformly refined meshes of approximately 2×10^5, 4×10^5, and 8×10^5 cells showed that a discrepancy between shock wave coordinates obtained on the second and third meshes did not exceed 1%. Global time steps of 5×10^{-7} s and 10^{-6} s yielded indistinguishable solutions. For this reason, the time step of 10^{-6} s and mesh of 4×10^5 cells were employed for the study of 2D flow structure and stability at various M_∞ and α. The root-mean-square CFL number (over mesh cells) was about 2.

3D flow simulations were performed for a channel created by an extrusion of the profile depicted in Fig. 1 from the plane $z=0$ to $z=\pm30$. Details of the mesh and boundary conditions are given in Section 6.

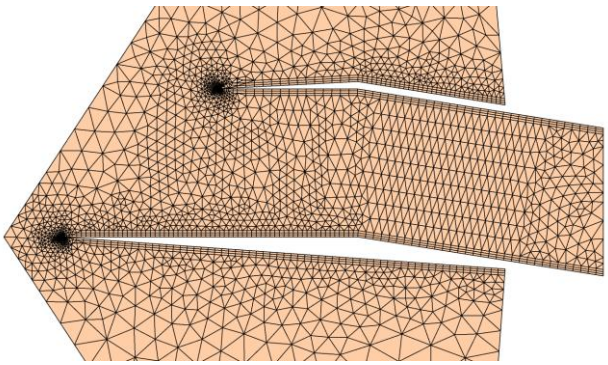

Fig. 2 Schematic of the computational mesh

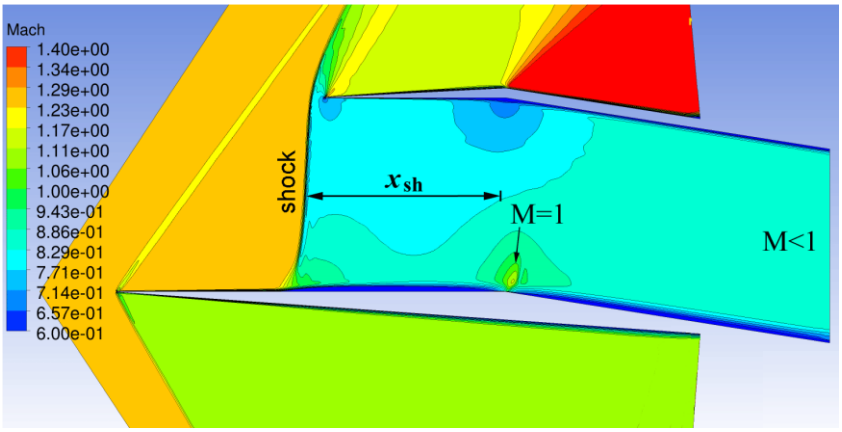

Fig. 3 Mach number contours and expelled shock wave at α=0, M_∞=1.28, M_{exit}<1, p_{exit}=65,000 N/m^2

The solver was validated by computation of several benchmark 2D and 3D problems. For instance, we simulated transonic flow past a Busemann biplane of length l=1, height h=0.5, and wedge thickness of 0.05 (Kuzmin 2017). The calculated shock positions and drag coefficient were undistinguishable from numerical data obtained by Maruyama *et al*. (2009) and Hu *et al*. (2011).

4. Shock position as a function of M_∞ at zero angle of attack and subsonic exit

First, we solved the problem at M_∞=1.28 using the subsonic exit condition with p_{exit}=65,000 N/m^2. The free stream (3) was employed for initialization of the solution. Computations showed a convergence of the mean parameters of turbulent flow to a steady state in less than 0.1 s of physical time. The obtained flow field exhibits a small local supersonic region over the bend of lower wall, see Fig. 3. A nearly normal shock is formed in front of the entrance x=−28, 0<y<30. Such a flow pattern is called hereafter the flow regime with an expelled shock. To analyze streamwise positions of the shock, we will trace its x-coordinate x_{sh} at the height y=15.

After calculation of the flow at M_∞=1.28, we solved the problem for M_∞=1.29, 1.295, and 1.296. At each step, for initial conditions we used the flow field obtained at the previous M_∞. The lower branch of curve 1 in Fig. 4 shows that, in this band of M_∞, the shock coordinate x_{sh} changes insignificantly. Further increase of M_∞ to 1.30 triggers a swallowing of the shock wave, i.e., a jump

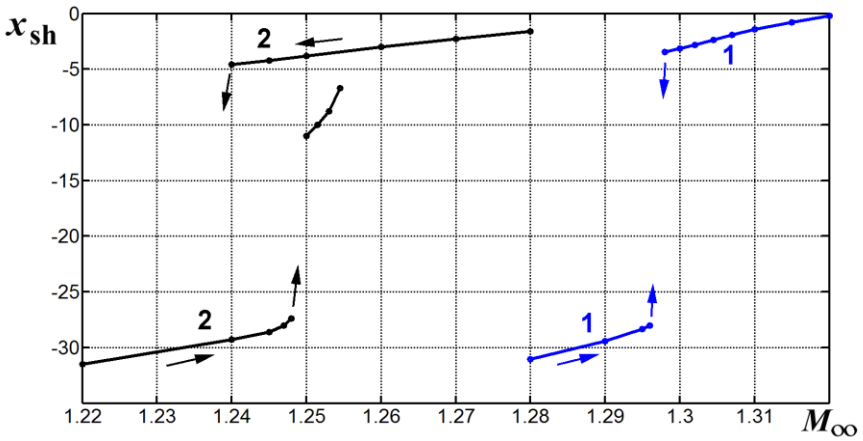

Fig. 4 Coordinate x_{sh} of the shock versus M_∞ at α=0 and subsonic exit: 1 – p_{exit}=65,000 N/m^2, 2 – p_{exit}=55,000 N/m^2. The upper (lower) branches of the curves correspond to flow regimes with the swallowed (expelled) shock

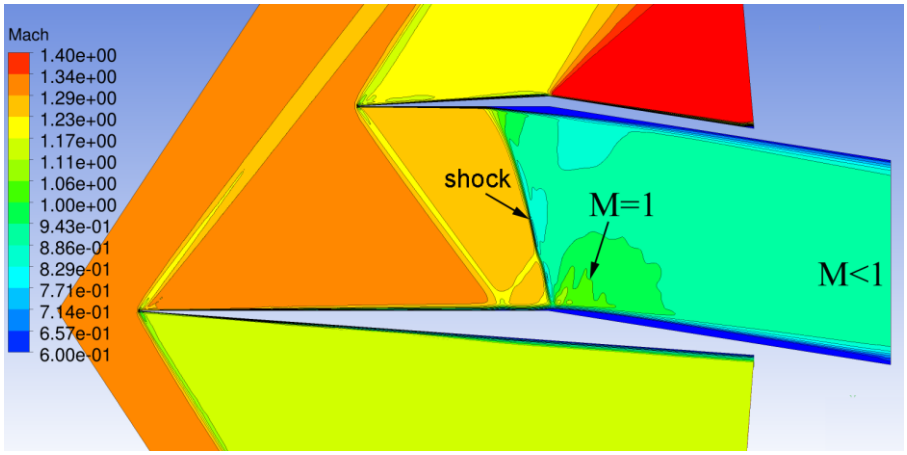

Fig. 5 Mach number contours at α=0, M_∞=1.3, M_{exit}<1, p_{exit}=65,000 N/m^2

of the shock downstream from the entrance to the bend of channel (Fig. 5). This means a transition from the lower branch of curve 1 in Fig. 4 to the upper one. After that an increase of M_∞ from 1.30 to 1.32 yields a shift of the shock downstream and expansion of the supersonic region over the bend of lower wall. The obtained flow is nearly uniform at $x< -13$, exhibiting only weak perturbations generated by the leading edges of both walls.

On the contrary, a decrease of M_∞ from 1.30 to 1.296 triggers a rupture of the supersonic region and expulsion of the shock from the channel. This means a transition from the upper branch of curve 1 in Fig. 4 to the lower one.

In the same way we calculated a dependence $x_{sh}(M_\infty)$ for p_{exit}=55,000 N/m^2. In the band $1.30<M_\infty<1.32$, the smaller p_{exit} yields an essential displacement of the swallowed shock downstream to the channel exit. Therefore one needs smaller M_∞ to return the shock foot to a position near the lower wall bend, which admits a rupture of the supersonic region and shock expulsion due to a small perturbation. That is why curve 2 in Fig. 4 is shifted to smaller M_∞ with

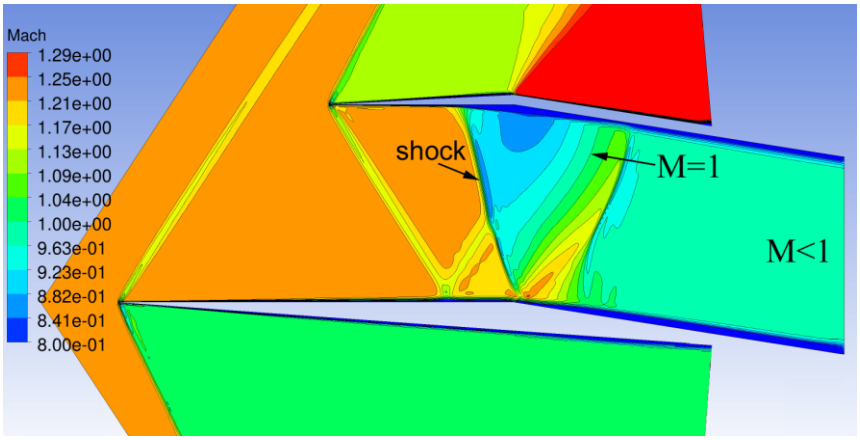

Fig. 6 Mach number contours at α=0, M_∞=1.24, M_{exit}<1, p_{exit}=55,000 N/m^2. Flow regime corresponds to the upper branch of curve 2 in Fig. 4

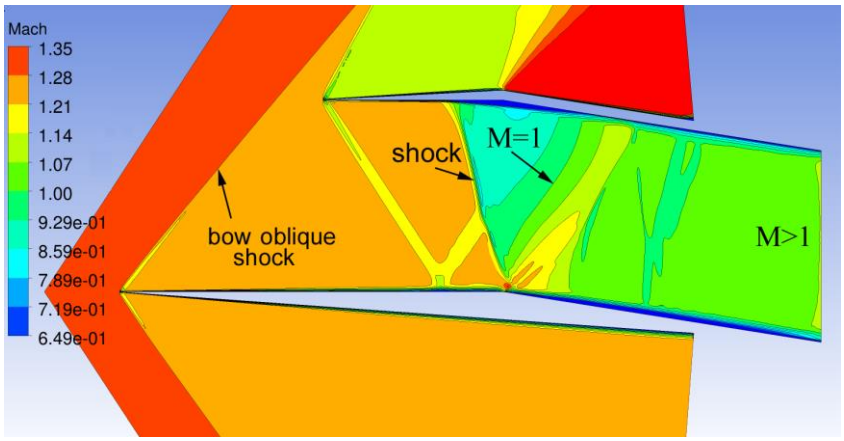

Fig. 7 Mach number contours at α= −2.5°, M_∞=1.34 and condition M_{exit} >1. Flow regime corresponds to the upper branch of curve 1 in Fig. 8

respect to curve 1. As seen, there is a hysteresis of curve 2, i.e., a dependence of x_{sh} values on the direction of change of M_∞. The existence of hysteresis is attributed to an enlargement of the supersonic region over the lower wall bend (Fig. 6) and, hence, stronger instability of the expansion flow/shock interaction as compared to the case p_{exit}=65,000 N/m^2.

Apart from the upper and lower branches, curve 2 exposes a short middle branch due to an interference of the perturbation generated by the leading edge of upper wall, since the perturbation delays the downstream shift of shock with increasing M_∞.

5. Shock position versus M_∞ at negative angles of attack

At negative angles α, the lower wall generates a bow oblique shock in addition to the shock formed due to the bend of channel, and the shock system configuration looks like to the one in a conventional intake with a forebody. Flow computations at α=−2.5°, 1.31<M_∞<1.36, p_{exit}=55,000

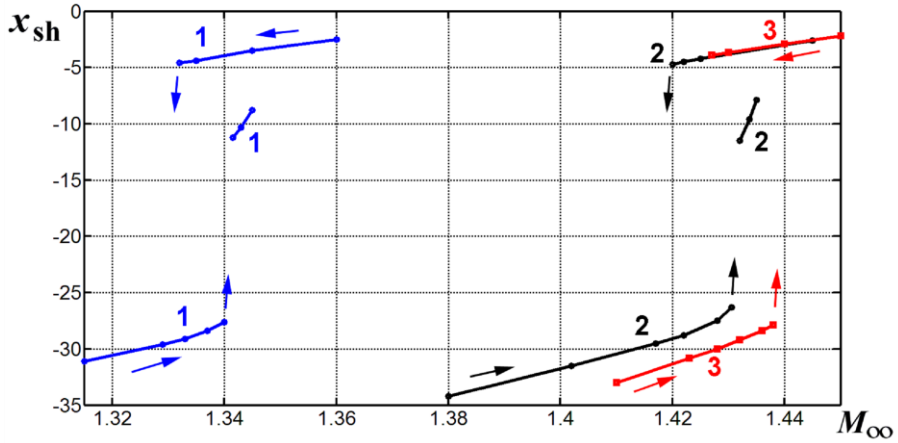

Fig. 8 Coordinate x_{sh} of the shock formed due to the bend of channel versus M_∞ at negative angles of attack: 1 – α=−2.5° and condition M_{exit}>1; 2 – α=−5° and M_{exit}>1; 3 – α=−5°, M_{exit}<1 and p_{exit}=75,000 N/m^2

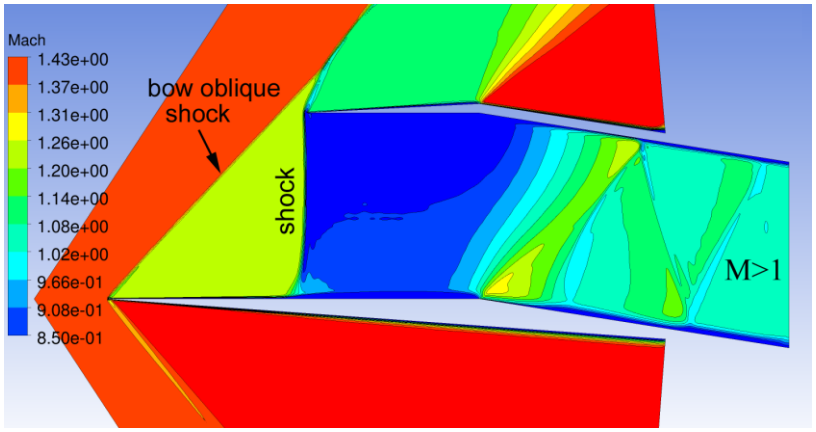

Fig. 9 Mach number contours at α=−5°, M_∞=1.425 and condition M_{exit}>1. Flow regime corresponds to the lower branch of curve 2 in Fig. 8

N/m^2 produced supersonic velocities at the channel exit; that is why we switched over to the boundary condition M_{exit}>1. Figure 7 shows that, between the bow shock and the entrance x=−28, 0<y<30, the flow is virtually uniform and parallel to the x-axis.

The position x_{sh} of shock formed due to the bend of channel is illustrated by curve 1 in Fig. 8. The drop of x_{sh} (indicating the shock expulsion from the channel) occurs when M_∞ becomes less than 1.332. We notice that at α=−2.5° the Mach number decreases across the bow oblique shock from M_∞=1.332 to M^*=1.239, and the latter remains constant in the region between the bow shock and entrance. This is in agreement with results obtained in Section 4. Indeed, the shock expulsion at α=0 and p_{exit}=55,000 N/m^2 occurs if M_∞ becomes less than 1.24, see curve 1 in Fig. 4. Instead of the bow shock, there is a weak perturbation generated by the leading edge of lower wall at α=0. The perturbation reduces the Mach number from 1.24 to the value of 1.233, which indeed agrees with M^*; the minor discrepancy is associated with different supersonic regions developed

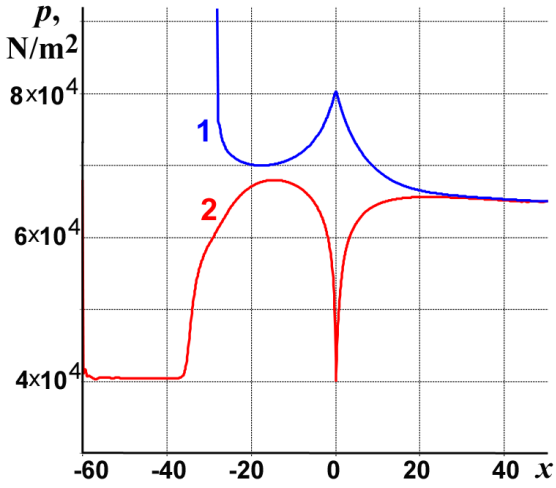

Fig. 10 Static pressure p on the walls in conditions of Fig. 3 (α=0, M_∞=1.28, M_{exit}< 1, p_{exit} = 65,000 N/m^2): 1 – upper wall, 2 – lower wall

downstream of the lower wall bend (see Fig. 6) and their influence the shock expulsion.

A decrease of α from −2.5° to −5° at 1.31<M_∞<1.36 results in strengthening the bow oblique shock, decreasing the Mach number behind it, and either shock expulsion from the channel or an upstream displacement of the expelled shock. Therefore, one needs a larger M_∞ to move the shock into the channel to a position admitting its interaction with the expansion flow over the lower wall bend. The calculated dependence $x_{sh}(M_\infty)$ at α= −5° is illustrated by curve 2 in Fig. 8. As seen from the upper branch of curve 2, the shock expulsion occurs when M_∞ becomes less than 1.42. We notice that the Mach number drops across the bow shock from 1.42 to 1.238, and this again agrees with the value 1.233 obtained in Section 4. Figure 9 illustrates Mach number contours at α=−5°, M_∞=1.425 in the regime with the expelled shock.

Another flow field in the channel at α= −5° was obtained by imposing the subsonic exit condition M_{exit}<1 along with the pressure p_{exit}=75,000 N/m^2. The calculated dependence of x_{sh} on M_∞ in this case is illustrated by curve 3. The narrower hysteresis band is explained by the smaller supersonic region formed over the lower wall bend.

6. Miscellanea

In all the cases examined, the flow field exhibits a boundary layer separation and subsequent reattachment near the upper wall bend where the flow is subsonic and, as a consequence, the pressure attains a local maximum, see curve 1 in Fig. 10. On the lower wall, a boundary layer separation occurs either upstream of the bend due to an adverse pressure gradient produced by the shock, or downstream of the bend due to a pressure rise incurred by the given p_{exit} at subsonic exit, see curve 2 in Fig. 10.

To study an effect of the Reynolds number Re, we performed computations at halved and doubled values of p_∞ which imply the halved and doubled Re, respectively. A comparison of curves 1 and 2 in Fig. 11 shows that the hysteresis band expands at the higher Re and, hence, thinner boundary layer. Inviscid flow computations showed further expansion of the hysteresis and disappearance of the middle branch in the dependence $x_{sh}(M_\infty)$, see curve 3.

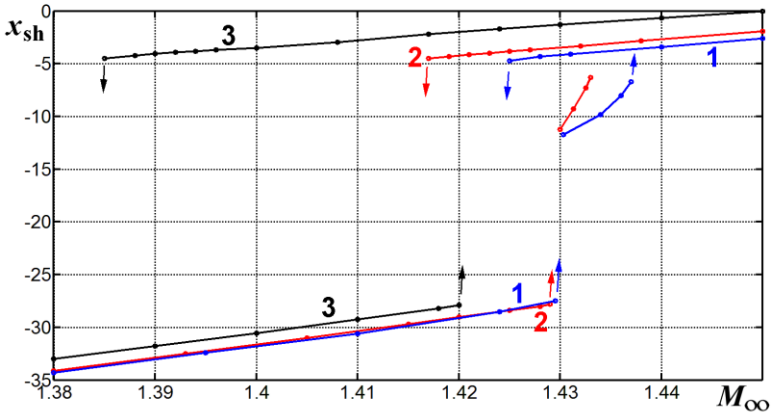

Fig. 11 Coordinate x_{sh} of the shock versus M_∞ at α=−5° and condition M_{exit}>1: 1 – p_∞=2×10^4 N/m^2, Re=3.1×10^5; 2 – p_∞=8×10^4 N/m^2 N/m^2, Re=12.5×10^5; 3 – inviscid flow

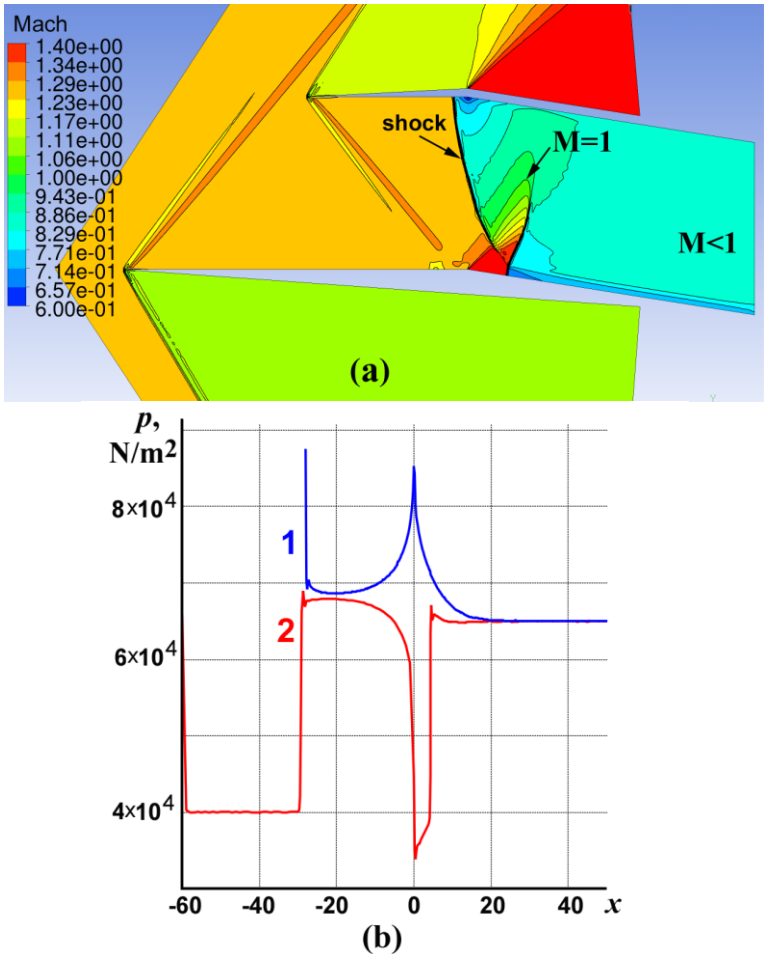

Fig. 12 Inviscid flow computations: (a) Mach number contours and a swallowed shock at M_∞=1.28, α=0, p_{exit}=65,000 N/m^2; (b) pressure on the walls in the regime with an expelled shock at M_∞=1.265, α=0, p_{exit}=65,000 N/m^2 (1 – upper wall, 2 – lower wall)

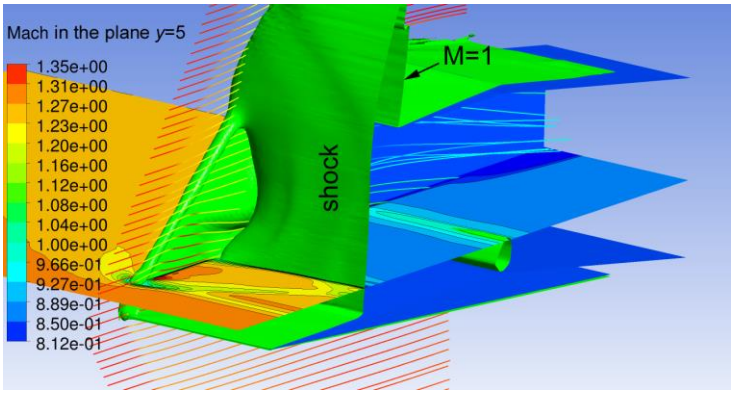

Fig. 13 Isosurfaces $M(x,y,z)=1$ in the 3D flow, Mach number contours in the horizontal plane $y=5$, and streamlines in a vicinity of the sidewall at $M_\infty=1.28$, $\alpha=0$, $M_{exit}<1$, $p_{exit}=65{,}000$ N/m^2

In the inviscid flow model, transitions between the upper and lower branches of the plots $x_{sh}(M_\infty)$ occur at smaller Mach numbers M_∞ than in turbulent one. For instance, at $\alpha=0$ and $M_\infty=1.28$, instead of an expelled shock (Fig. 3) computations demonstrated a flow field with a swallowed shock (see Fig. 12(a)) which looks similar to Fig. 4 obtained for turbulent flow at a larger $M_\infty=1.3$.

Inviscid flow with an expelled shock at $\alpha=0$ can only exist when $M_\infty\leq 1.27$. In this regime, pressure distributions on the walls are similar to those in turbulent flow, cf. Figs. 10 and 12(b). The pressure minimum in Fig. 12(b) corresponds to the velocity maximum located at $x=0.4$. Downstream of this point, at $0.4<x<4.25$, the velocity decreases in the local supersonic zone and pressure gradually rises. After that the pressure jumps to $p=7\times10^4$ N/m^2 due to a terminating shock wave.

A similar behavior of shocks was obtained in a channel whose upper wall is slightly shifted upstream with respect to the lower one. The shift produces a displacement of the hysteresis band to higher free-stream Mach numbers.

We notice that a larger thickness of the leading edges of the upper and lower walls results in the arising of extra local supersonic regions terminated by shocks, which may crucially change the shock system configuration (Kuzmin 2017).

A three-dimensional channel was created by an extrusion of the profile (1), (2) from the plane $z=0$ to $z=\pm30$. For CPU savings, we assumed the flow to be symmetric about the plane $z=0$ and solved the problem in the semi-channel at $z<0$. The sidewall of thickness 0.1 was located at $-30.1\leq z\leq-30$. The windward face of sidewall was a thin oblique rectangle extending from the upper wall to lower one. On the side boundary of the computational domain $z=-90$ we imposed the free-slip condition. A three-dimensional mesh was constituted by 1.7×10^6 prisms in 38 layers on the walls, with a sufficiently thin first layer to ensure $y^+<1$, and by about 16×10^6 tetrahedrons in the remaining region.

Figure 13 displays the expelled shock in front of the channel entrance and a weak shock in front of the sidewall at $M_\infty=1.28$, $\alpha=0$, i.e., in the same conditions as in Fig. 3. It can be seen that the distance between the shock and entrance in 3D flow is noticeably larger than the distance in 2D flow. Mach number contours in the plane $y=5$ demonstrate a sidewall perturbation that propagates towards the plane of symmetry and is reflected from it ahead of the entrance, decreasing the flow velocity in this region. The behavior of streamlines near the sidewall hints at a boundary layer

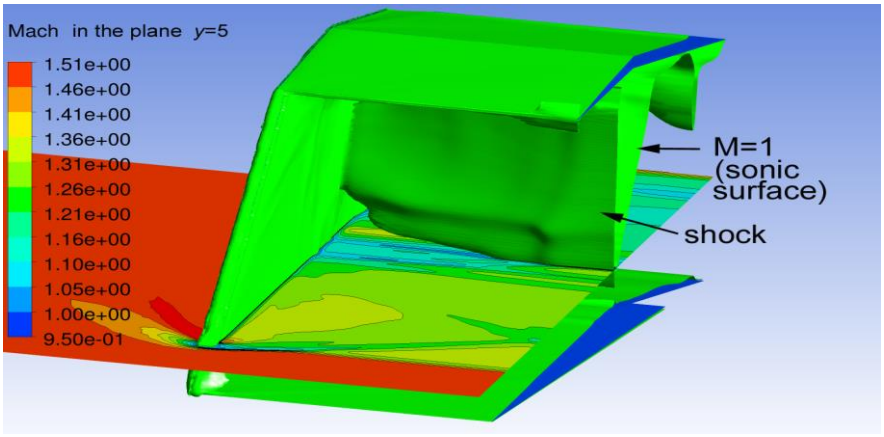

Fig. 14 Isosurfaces $M(x,y,z)=1$ in the 3D flow and Mach number contours in the plane $y=5$ at $M_\infty=1.5$, $\alpha=-5°$, $M_{exit}>1$.

separation from the sidewall in addition to separations from the upper and lower walls.

At a larger Mach number $M_\infty=1.5$ and negative α, the dependence of flow structure on the spanwise coordinate z becomes more essential. Near the symmetry plane $z=0$, the swallowed shock extends from the upper to lower wall, see Fig. 14, meanwhile at $z<-10$ it shrinks significantly. The bow shock generated by the lower wall is hidden in Fig. 14 to demonstrate Mach numbers in the plane $y=5$. The flow structure looks like a fin type flow (Panaras 1996, Knight *et al*. 2003, Nguyen *et al*. 2011) which implies a bow shock interaction with the sidewall shock that turns, compresses, and decelerates the near-wall flow.

3D effects produce an upstream displacement of the swallowed shock with respect to its position in the 2D flow. As a consequence, the rupture of supersonic region and shock expulsion in the 3D flow occur when M_∞ becomes less than 1.495 instead of 1.42 in 2D flow. That is why, for the channel under consideration, the shock position hysteresis is observed in the band $1.495\leq M_\infty \leq 1.56$ as compared to $1.42\leq M_\infty \leq 1.435$ in the 2D flow (see curve 2 in Fig. 8).

Thus, the 3D flow computations confirm the occurrence of flow hysteresis in the bent channel at angles of attack $-5°\leq\alpha\leq 0$, though the presence of sidewall influences considerably the flow field, except for a vicinity of the symmetry plane. With increasing Reynolds number or span of channel, the influence of sidewall is expected to decrease. A detailed analysis of flow features in a bent 3D channel will be done in a subsequent paper.

7. Conclusions

Numerical simulations of 2D transonic flow in the bent channel demonstrated abrupt changes of shock wave positions under gradual variations of the free-stream Mach number at zero or negative angles of attack. The instability is attributed to the expansion flow/shock-wave interaction near the convex bend of lower wall. The shock position as a function of the free-stream Mach number usually exhibits hysteresis, whose width depends on the given boundary conditions. The width is larger in flow regimes with the supersonic exit comparing to subsonic one. Simulations of the 3D flow in a channel of semi-span equal to the height produced reasonable results which agree with the findings obtained for the 2D flow.

Acknowledgment

This research was performed using computational resources provided by the Computational Center of St. Petersburg State University (http://cc.spbu.ru).

References

Feng, S., Chang, J., Zhang, Ch., Wang, Y., Ma, J. and Bao, W. (2017a), "Experimental and numerical investigation on hysteresis characteristics and formation mechanism for a variable geometry dual-mode combustor", *Aerosp. Sci. Technol.,* **67**, 96-104.

Feng, S., Chang, J., Zhang, Y., Zhang, Ch., Wang, Y. and Bao, W. (2017b), "Numerical studies for performance improvement of a variable geometry dual mode combustor by optimizing deflection angle", *Aerosp. Sci. Technol.,* **68**, 320-330.

Guo, S., Wang, Z. and Zhao, Y. (2014), "The flow hysteresis in the supersonic curved channel", *J. Natl. U Defense Technol.*, **36**(4), 10-14.

Han, J.A., Zhong, J.J., Yan, H.M., Sun, P. and Yu, Y. (2009), "Numerical research of three dimensional flow-path in a ram-rotor", *J. Aerosp. Power*, **24** (5), 1079-1088.

Hu, R., Jameson, A. and Wang, Q. (2011), "Adjoint based aerodynamic optimization of supersonic biplane airfoils", *J. Aircraft*, **49**(3), 802-814.

Kang, W., Liu, Zh., Lu, J., Wang, Yu and Dong, Y. (2014), "A numerical study for flow excitation and performance of rampressor inlet considering rotor motion", *Shock Vib.*, **2014**.

Knight, D., Panaras, A.G. and Zheltovodov, A.A. (2003), "Advances in CFD prediction of shock wave turbulent boundary layer interactions", *Progress Aerosp. Sci.*, **39**(2), 121-184.

Kotteda, V.M.K. and Mittal, S. (2016), "Flow in a Y-intake at supersonic speeds", *J. Propulsion Power*, **32** (1), 171-187.

Kuzmin, A. (2015), "Shock wave instability in a channel with an expansion corner", *J. Appl. Mech.*, **7**(2), 1550019.

Kuzmin, A. (2016), "Shock wave bifurcation in channels with a bend", *Arch. Appl. Mech.*, **86**(5), 787-795.

Kuzmin, A. (2017), "Transonic flow instability in the entrance region of a channel with breaks of walls", *Arch. Appl. Mech.*, **87**(8), 1269-1279.

Menter, F.R. (2009), "Review of the Shear-Stress Transport turbulence model experience from an industrial perspective", *J. Comput. Fluid Dynam.*, **23**(4), 305-316.

Maruyama, D., Kusunose, K. and Matsushima, K. (2009), "Aerodynamic characteristics of a two-dimensional supersonic biplane, covering its take-off to cruise conditions", *Shock Waves*, **18**(6), 437-450.

Nguyen, T., Behr, M. and Reinartz, B.U. (2011), "Numerical investigations of the effects of sidewall compression and relaminarization in 3D scramjet inlet", *the 15th AIAA International Space Planes and Hypersonic Systems and Technologies Conference,* Ohio, U.S.A., April.

Panaras, A.G. (1996), "Review of the physics of swept-shock/boundary layer interactions", *Prog. Aerosp. Sci.*, **32**(2-3), 173-244.

Sforza, P.M. (2012), *Theory of aerospace propulsion*, Academic Press, Waltham, Massachusetts, U.S.A.

Spalart, P.R. and Shur, M. (1997), "On the sensitization of turbulence models to rotation and curvature", *Aerosp. Sci. Technol.*, **1**(5), 297-302.

Torenbeek, E. and Wittenberg, H. (2009), *Flight Physics*, *Essentials of Aeronautical Disciplines and Technology with Historical Notes*, Springer, Dordrecht, The Netherlands.

EC